SOILS AND FOUNDATIONS Vol. 33, No. 1, 155-168, Mar. 1993
Japanese Society of Soil Mechanics and Foundation Engineering

LIMIT ANALYSIS OF WEAK LAYERS UNDER EMBANKMENTS

RADOSLAW L. MICHALOWSKI[i)]

ABSTRACT

Limit loads on finite layers of weak soil over a rigid base are analyzed using the upper bound approach. The soil is considered cohesive, and the Tresca yield condition is used to describe its strength. Strength increasing with depth is considered, and different strengths of the base interface are accounted for. The analysis is performed having the design of embankments in mind, and it makes it possible to account for the arbitrary horizontal component of the load generated by the horizontal thrust in the embankment. Results are compared to the lower bound solutions of particular cases available in the literature. Even though the upper bound approach was used, the solutions presented fall very close to the lower bound solutions. The advantage of the solutions presented in this paper is in easier calculations of bearing capacity, especially when the soil strength increases with depth, and in accounting for the arbitrary horizontal load transmitted from the embankment to the foundation soil. A proposal for arriving at critical heights of both unreinforced and reinforced embankments is given.

Key words: bearing capacity, embankments, limit state design, plasticity, weak soils (**IGC**: E3)

INTRODUCTION

The resultant load on the foundation soil from embankments is vertical and equal to the weight of the fill; however, the outward-acting tangential load (with a zero integral over the entire embankment width) is caused by the horizontal thrust in the embankment. During failure of the foundation soil, this outward load continues to exist, as the embankment is free to "spread" laterally, following the displacements of the foundation soil. These outward horizontal forces have an adverse effect on the bearing capacity, as opposed to the inward forces resisting failure under rough footings. Application of bearing capacity solutions for footings which, at best, assume no tangential stress on the interface (smooth footings) is then expected to be unsafe in unreinforced embankment design. The adverse effect of the horizontal outward load can be prevented by placing reinforcement at the bottom of the embankment fill (see, e.g., Jewell 1988). This paper considers the bearing capacity of a weak layer subjected to an arbitrary horizontal load component, characteristic of unreinforced and reinforced embankments.

The bearing capacity of a finite thickness layer was first considered by Jürgenson (1934), and a substantial contribution can be found in a paper by Mandel and Salençon (1972). The bearing capacity of cohesive layers with strength increasing with depth was later analyzed by Matar and Salençon (1977). Both papers

[i)] Department of Civil Engineering, The Johns Hopkins University, Baltimore, MD 21218, USA.
Manuscript was received for review on February 7, 1992.
Written discussions on this paper should be submitted before October 1, 1993 to the Japanese Society of Soil Mechanics and Foundation Engineering, Sugayama Bldg. 4 F, Kanda Awaji-cho 2-23, Chiyoda-ku, Tokyo 101, Japan. Upon request the closing date may be extended one month.

employ the method of characteristics to solve the set of hyperbolic equations describing the stress field in the layer. Even though these solutions were meant as the bearing capacity of layers under footings, they are used in most design techniques for embankments over soft soil layers (e.g., Silvestri 1983, Bonaparte et al. 1987, and Rowe and Soderman 1987). The solution to the entire boundary value problem is shown in Fig. 1 for rough interface DO′. It starts with the Cauchy problem in triangle ABC, followed by the solution in area BCDE with a singular point at B. The last characteristic of fan BCDE coincides with interface BE. Hence, the limit load along BE has an inward horizontal component of intensity equal to the soil cohesion. The same is true along EG, where point G is found from the condition that characteristic GJ must approach line OO′ at angle $\pi/4$ (symmetry condition). The intensity of the horizontal load along OG is not known, but it can be estimated from extending the plastic region into GJO. This intensity drops to zero at point O.

The assumption of inward-acting horizontal forces, quite appropriate for rough footings, leads to a significant overestimation of the bearing capacity if applied to unreinforced embankments, where the shear stress on the foundation soil is of the opposite sign. It should be emphasized that the solutions by Mandel and Salençon and by Matar and Salençon were not intended by those authors to describe the bearing capacity under unreinforced embankments, and the correctness of these solutions is not questioned. Only the extension of the applicability of these solutions to unreinforced embankments is disputed.

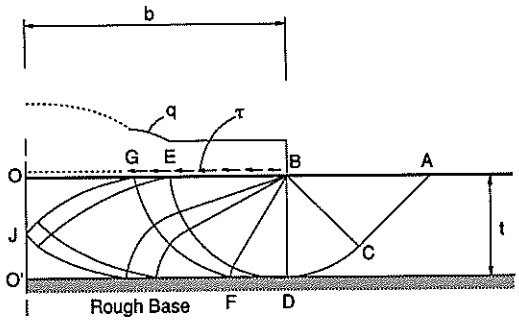

Fig. 1. Stress characteristics field in the solution of the bearing capacity of a rough footing over a layer on a rough base, Mandel and Salençon (1972)

A different approach to estimating the bearing capacity of weak layers under embankments was offered by Leshchinsky (1987). This approach is based on a rotational mechanism of failure. While such a mechanism is very effective in analyzing the failure of embankment slopes (Leshchinsky, 1987), its extension to modeling failure under the entire embankment leads to bearing capacities which are higher than those based on the collapse mechanisms proposed in this paper, especially for wide embankments or thin layers (as both estimates are upper bounds, the lower one is more reliable). An approximate approach based on the differential slice technique was proposed by Jewell (1988). Analyses of the bearing capacity of a weak soil of unlimited thickness under loads with arbitrary horizontal components were presented by Houlsby and Jewell (1988) and Michalowski (1992).

An extensive study of case histories of embankments over soft soils was conducted by Humphrey and Holtz (1986). They found that predictions of embankment heights based on the classical Prandtl solution ($H=5.14c/\gamma_f$) considerably underestimate the true critical value, and they concluded that the limited thickness of the weak foundations and the increase of strength with depth (which is usually the case) are likely to be among the factors responsible for critical heights larger than expected. Both strength increase with depth and foundation thickness are accounted for in the solutions presented in this paper.

The solutions in this paper are obtained using the upper bound approach of limit analysis (Drucker et al., 1952). The limit stress state of the soil is described by the Tresca yield condition (with the undrained shear strength being the material parameter), which is a generally accepted failure criterion for normally consolidated cohesive soils under undrained conditions. The flow rule is assumed to be associative. The upper bound theorem can be expressed as follows: the rate of work done by the external forces (tractions and material weight) is less or equal to the energy dissipa-

tion rate in any kinematically admissible failure mechanism. Hence, equating the rate of external work to internal dissipation allows one to calculate the upper bound to the true limit load. The flow rule associated with the Tresca yield condition leads to a velocity field with incompressible deformation. It also implies that a velocity jump vector across a velocity discontinuity considered as a nonelongating line is constant and tangent to that discontinuity. The term "velocity jump vector" will be used throughout the paper to describe the difference in velocity of neighboring particles separated by a velocity discontinuity (failure surface).

The mechanisms of failure of a soil layer under an embankment considered in this paper are presented in the next section. In the following sections the bearing capacity of a layer under an embankment is analyzed for cases of homogeneous soil and soil with strength increasing with depth. Next, a more approximate closed-form solution is presented. Application of the results is then shown for finding critical heights of embankments, including the influence of reinforcement. The conclusions are presented in the last section.

MECHANISMS OF FAILURE

Three kinematically admissible collapse mechanisms of a layer over a rigid base are shown in Figs. 2(a), 3(a), and 3(c). All three are plane-strain mechanisms, as the length of the load (embankment) is considered large with respect to the width.

The first mechanism, Fig. 2(a), is similar to that associated with the static solution proposed by Hill (1950), with its depth restricted by the thickness of the layer. Length AE is equal to half of the width of the load (half of the embankment width). Vertical component V^0 of the velocity along AE is a given boundary condition. Block ABE then moves as a rigid body with velocity V_{ABE} (see hodograph in Fig. 2(b)), whose vertical component is equal to V^0, area BCE undergoes continual deformation, and block CDE moves as a rigid body. The two other mechanisms (Figs. 3(a) and 3(c)) are very different from the first one, in that the part of the layer immediately under the load is divided into more rigid-motion blocks, some of which slide over the rigid base. The number of blocks increases with an increase in ratio b/t. These mechanisms are similar to those adapted in the limit analysis of the compression of metal blocks between rigid platens (e.g., Collins 1969) and those used by Izbicki and Mróz (1976) to analyze limit loads on soil layers. The vertical velocity component of boundary OBD is, again, considered a bound-

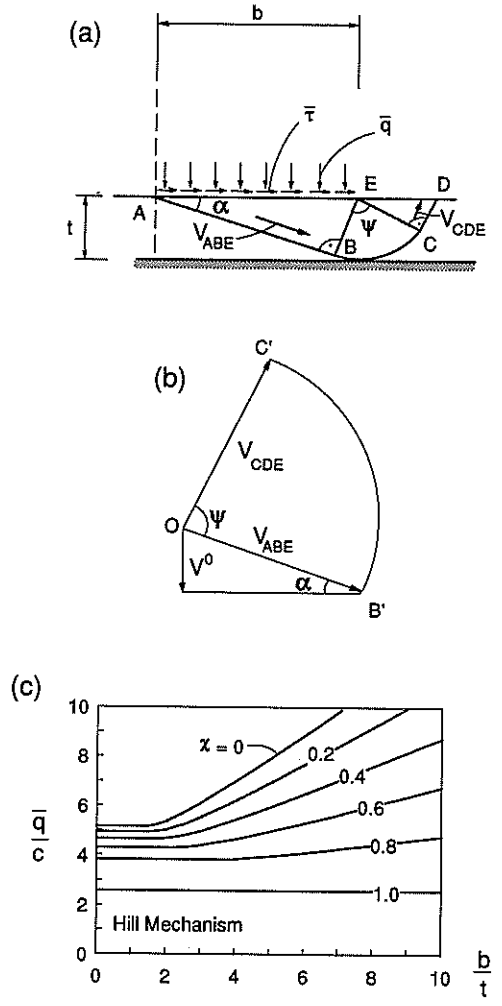

Fig. 2. (a) Symmetrical half of the Hill-type failure mechanism; (b) hodograph; (c) limit value of $\bar{q}/c$ for different outward shear stress mobilization on the foundation soil; homogeneous soil

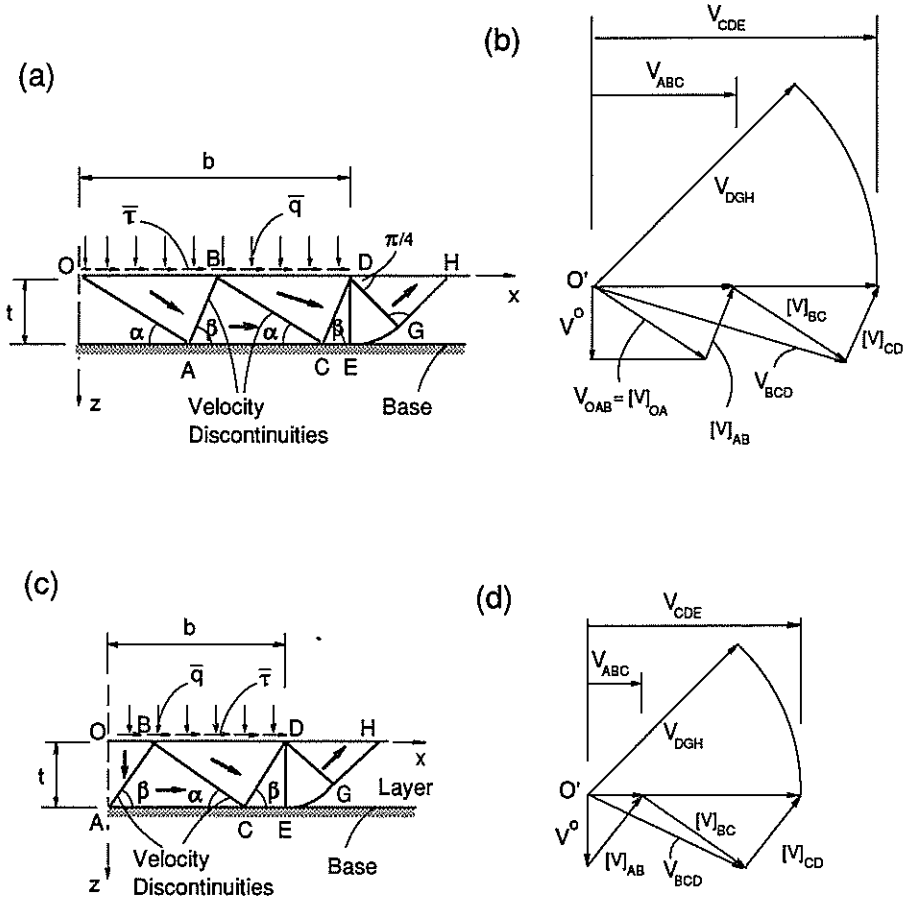

Fig. 3. (a), (c) Collapse mechanisms of a layer; (b), (d) hodographs

ary condition. The rigid blocks in the mechanism shown in Fig. 3(a) are separated by velocity discontinuities OA, AB, BC, and CD. Velocities of particular blocks are represented on the hodograph (Fig. 3(b)), where the velocity jumps across discontinuities are indicated by brackets. Only area EGD undergoes continual deformation. Interfacial failure is assumed to take place along the base (ACE). The mechanism in Fig. 3(c) is similar to that in Fig. 3(a); however, here, the middle block, OAB (symmetrical half), is considered to move down vertically.

The limit load is assumed to be distributed along surface OBD (Figs. 3(a) and 3(c)). The horizontal load component is given as a fraction of the undrained shear strength at the surface of the layer, $\bar{\tau}=\chi c$ (χ in the range of -1 to 1, the limit values representing fully mobilized inward and outward shear stress, respectively). $\bar{\tau}$ is then a stress boundary condition.

Angles α and ψ in the first mechanism, and angles α and β in the other two, must be such that the mechanisms are kinematically admissible. Their particular values will be determined from a minimization scheme where the minimum of the limit load, $\bar{q}$, is sought.

HOMOGENEOUS LAYER OVER SMOOTH AND ROUGH BASES

Fig. 2(c) represents results based on the analysis of the failure mechanism shown in Fig. 2(a). The average limit pressure $\bar{q}/c$ is

shown as a function of ratio b/t (half-width/layer thickness) for different horizontal load coefficients χ ($\chi=\bar{\tau}/c$). This mechanism is forced to a depth not exceeding the thickness of the layer, and the solution can be presented as (Michalowski, 1992)

$$\frac{\bar{q}}{c}=2\psi+(1-\chi)\cot\alpha+\cot(\psi-\alpha) \qquad (1)$$

where angles α and ψ are found from a minimization procedure of $\bar{q}/c$ with the condition: $\sin\alpha\leq t/b$. For a half-space (infinitely thick layer), the minimum was found analytically when $\psi=\pi/4+\alpha$ and $\alpha=(\arccos\chi)/2$, hence

$$\frac{\bar{q}}{c}=1+\frac{\pi}{2}+\arccos\chi+\sqrt{1-\chi^2} \qquad (2)$$

This solution, though obtained in a different form and using the method of characteristics, was obtained earlier by Sokolovski (1965). Eq. (2) describes the horizontal portions of the lines in Fig. 2(c), where the base of the layer does not interfere with the failure mechanism, while the inclined parts were obtained from Eq. (1), where $\psi=\pi/4+\alpha$ and $\alpha=\arcsin(t/b)$ to yield

$$\frac{\bar{q}}{c}=1+\frac{\pi}{2}+2\arcsin\left(\frac{t}{b}\right)+(1-\chi)\sqrt{\left(\frac{b}{t}\right)^2-1} \qquad (3)$$

Eq. (3) overestimates the true limit loads, particularly for smooth bases (the limit loads from such analysis are independent of whether the base is smooth or rough).

The failure mechanisms leading to more realistic upper bounds for large ratios b/t are those in Figs. 3(a) and 3(c). Only the analysis based on the first mechanism, Fig. 3(a), will be presented in detail, while the numerical results shown will be based on both mechanisms. Depending on ratio b/t, the number of blocks in the mechanism changes. The number of moving blocks under the loaded surface is taken as the characteristic number n. For the mechanism in Fig. 3(a), $n=4$. Note that n can assume only even natural values.

The upper bound theorem can be written as

$$\int_v \dot{\varepsilon}_{ij}^k\sigma_{ij}\,dv+\int_L c[V]_l^k\,dL+\int_{Lb} c_b[V]_b^k\,dL_b\geq\int_S Q_i V_i\,dS+\int_v \gamma_i V_i^k\,dv, \quad i,j=1,2,3 \qquad (4a)$$

or

$$\dot{D}_v+\dot{D}_L+\dot{D}_{Lb}\geq\dot{W}_Q+\dot{W}_\gamma \qquad (4b)$$

where superscript k denotes a strain-rate and velocity fields related to the kinematically admissible mechanism. The first term on the left-hand side represents the work dissipation rate in the continually deforming area ($\dot{\varepsilon}_{ij}^k$ being the strain rate tensor and σ_{ij}-the stress tensor), and the second and third terms represent the dissipation rates along discontinuities within the layer and along the base, respectively (c_b-the shear strength of the base interface). The two terms on the right-hand side represent the work rate of external load Q_i (stress vector with components $\bar{q}$ and $\bar{\tau}$) and the work rate related to displacement of the soil, γ_i being the vector of unit weight. Due to the incompressibility of the material, the last term in Eq. (4) is equal to zero (a direct consequence of the mass conservation principle). The energy dissipation rate along a velocity discontinuity surface of length l within a cohesive material (per unit width) is

$$\dot{d}=l[V]c \qquad (5)$$

where $[V]$ is the magnitude of the velocity jump vector and c is the cohesion. Velocity jumps across discontinuities OA, BC, and AB and CD in Fig. 3(a) are $V^0/\sin\alpha$ and $V^0/\sin\beta$, respectively. The velocity jump across discontinuity EGH is $V_0 n(\cot\alpha+\cot\beta)/2$. The dissipation rate within all discontinuities within the layer then becomes

$$\dot{D}_L=\frac{ntV^0}{2\sin^2\alpha}c+\frac{ntV^0}{2\sin^2\beta}c+\frac{n\pi tV^0}{8}(\cot\alpha+\cot\beta)c+\frac{ntV^0}{2}(\cot\alpha+\cot\beta)c \qquad (6a)$$

where the four terms represent dissipation rates along discontinuities inclined at angle α to the horizontal, along those inclined at angle β to the horizontal, and dissipation along EG, and GH, respectively. Eq. (6a) can be rewritten as

$$\dot{D}_L=\frac{n}{2}V^0tc\left[\frac{1}{\sin^2\alpha}+\frac{1}{\sin^2\beta}+\left(\frac{\pi}{4}+1\right)(\cot\alpha+\cot\beta)\right] \tag{6b}$$

where n describes the number of moving blocks under the loaded surface. Dissipation within area DGE is

$$\dot{D}_v=\int_v \sigma_{ij}\,\dot{\varepsilon}^k_{ij}\,dv=\int_0^t\int_0^{\pi/4}\frac{V^0}{2}\,n(\cot\alpha+\cot\beta)c\,d\theta\,dr=\frac{n\pi}{8}V^0tc(\cot\alpha+\cot\beta) \tag{7}$$

The velocity jump vector along base AC is equal to the velocity of block number 2 (ABC), and is equal to $V_0(\cot\alpha+\cot\beta)$, and the velocity along CE (block number 4) is twice as large. For a mechanism with an arbitrary even number n, these velocities become: $V_0(\cot\alpha+\cot\beta)i/2$, where $i=2, 4, \cdots n$. The rate of energy dissipation along the base then becomes

$$\dot{D}_{Lb}=tV_0(\cot\alpha+\cot\beta)^2c_b\frac{1}{2}\sum_{i=1}^{n-2}i+\frac{1}{2}ntV^0\cot\beta(\cot\alpha+\cot\beta)c_b,\quad i=2, 4, 6\cdots n-2 \tag{8a}$$

where the first term describes the dissipation rate along base interface AC (in general, for $n>4$, there are more blocks similar to ABC sliding over the base interface), and the second term describes the dissipation along CE. Eq. (8a) can be written in a more convenient form

$$\dot{D}_{Lb}=\frac{n}{8}V^0tc_b(\cot\alpha+\cot\beta)[(n-2)\cot\alpha+(n+2)\cot\beta] \tag{8b}$$

The strength of the base interface, c_b, is a fraction of the shear strength of the soil, $c_b=\kappa c$ (κ in the range from 0 to 1.0, i.e., smooth to perfectly rough). The work of external forces on OBD is split into two parts: the work of the unknown vertical load $\bar{q}$

$$\dot{W}_q=\bar{q}bV^0 \tag{9}$$

and the work of the known, uniformly distributed, horizontal load $\bar{\tau}$. Horizontal components of velocities of blocks OAB (block number 1) and BCD (block number 3) can be written in general as $V^0[(i+1)\cot\alpha+(i-1)\cot\beta]/2$, where $i=1, 3, 5\cdots n-1$. The rate of work of $\bar{\tau}$ becomes

$$\dot{W}_\tau=t(\cot\alpha+\cot\beta)\bar{\tau}\sum_{i=1}^{n-1}V^0[(i+1)\cot\alpha+(i-1)\cot\beta]/2,\quad i=1, 3, 5\cdots n-1 \tag{10a}$$

or

$$\dot{W}_\tau=\frac{n\chi}{8}V^0tc(\cot\alpha+\cot\beta)[(2+n)\cot\alpha+(n-2)\cot\beta] \tag{10b}$$

where χ is the coefficient describing the intensity of the horizontal load as a fraction of the shear strength of the layer, $\bar{\tau}=\chi c$ ($-1.0\le\chi\le1.0$). An expression for the upper bound to $\bar{q}$ can be obtained after substituting Eqs. (6)–(10) into Eq. (4) and solving for $\bar{q}$. The average dimensionless limit load $\bar{q}/c$ obtained is independent of the true distribution of q, as the vertical velocity component of the loaded boundary is constant (thus the work-rate of this load is independent of its distribution). The resulting expression is a function of α, β, and the characteristic number n. Solid lines in Fig. 4 were obtained from this expression, where α and n were varied (β is a dependent parameter when b/t is given) to obtain a minimum value of $\bar{q}$ (bullets in Fig. 4 are from

an analytical solution presented later). The diagrams are shown for smooth, "semi-rough" (base strength equal to half of the soil strength, $\kappa=0.5$), and perfectly rough bases, and for different factors χ representing different intensities of the outward horizontal load on the layer (characteristic of unreinforced embankments; diagrams for $\chi<0$, applicable to reinforced embankments, are presented later in the paper). While angle α can vary continuously within the admissible range, the value of n can assume only even numbers (2, 4, 6$\cdots$). For each value of b/t calculations were performed for all reasonable values of n, and for each n the minimum of $\bar{q}$ was found with angle α being the variable. Then, the least minimum was selected as the best upper bound estimate. Characteristic "waves" in the diagrams in Fig. 4 can be seen for small ratios b/t. These are due to an abrupt change in number n, which assures the minimum value of $\bar{q}/c$. The number n for which the minimum of $\bar{q}/c$ is found increases with an increase in b/t. A change in n leads to a change in the geometry of the mechanism, and, consequently, to a change in the derivative of curves calculated in Fig. 4 (the curves were smoothed by the plotting program). For large b/t, these fluctuations become insignificant. For small ratios b/t (thick layers), the minimum limit load $\bar{q}/c$ is obtained from the Hill mechanism (Fig. 2(a)), and this load is independent of b/t (horizontal portions; the base of the layer does not interfere with the failure mechanism). Limit load $\bar{q}/c$ is very sensitive both to the intensity of the horizontal load and to the strength of the base interface.

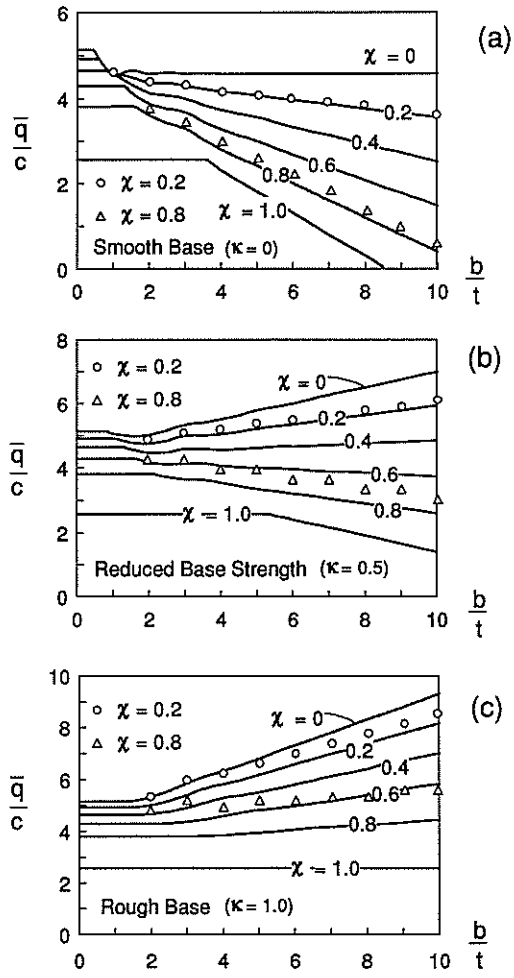

Fig. 4. Dimensionless limit load $\bar{q}/c$ for outward horizontal loads on the foundation layer, homogeneous soil: (a) smooth base; (b) base interface strength equal to half of the shear strength of the soil; (c) perfectly rough base. Solid lines indicate the numerical solution and bullets mark the closed-form solution

The least limit load is obtained for a smooth interface, where, for no horizontal load condition ($\chi=0$), limit load $\bar{q}/c$ becomes constant for larger b/t and equal to 4.57 (or $3+\pi/2$). Once the horizontal load due to the thrust in the embankment increases (increase in χ), the limit load drops down, and, theoretically, reaches zero for sufficiently large ratios b/t. Here, the smooth base interface acts as a "weakening" surface whose adverse effect becomes more pronounced while its relative depth becomes smaller (large b/t). This result is not surprising, since, for a layer thickness reaching zero, not even a small horizontal load can be supported (smooth interface). The limit loads are influenced significantly by the strength of the base interface, reaching the maximum for a perfectly rough base where the shear strength (c_b) is assumed to be equal to that of the soil. As opposed to smooth bases, limit load $\bar{q}/c$ for rough bases increases with

an increase in b/t.

STRENGTH INCREASING WITH DEPTH

The influence of strength increasing with depth was accounted for by Davis and Booker (1973) for unlimited thickness weak cohesive soils, and by Matar and Salençon (1977) for layers, using the method of characteristics. An upper bound analysis is performed here for layers where the shear strength increases linearly with depth z

$$c=c_m+\xi z \tag{11}$$

where c_m is the shear strength at the surface, and ξ is the gradient of the strength with depth. Energy dissipation rates are calculated taking the increased shear strength into account. Since the velocity jump vector along each discontinuity is constant, the dissipation rate along each discontinuity is calculated taking into account the shear strength at its centroid. The dissipation rate within the continually deforming area is calculated as presented earlier (Michalowski, 1992). The diagrams in Fig. 5 represent the limit loads calculated for dimensionless coefficient $\xi b/c_m=5$. The solid lines represent the numerical solution, where the minimum of $\bar{q}/c_m$ was sought. The horizontal portions of the lines come from analysis of the Hill mechanism. Depending on the base strength and horizontal load, $\bar{q}/c_m$ may increase or decrease with ratio b/t.

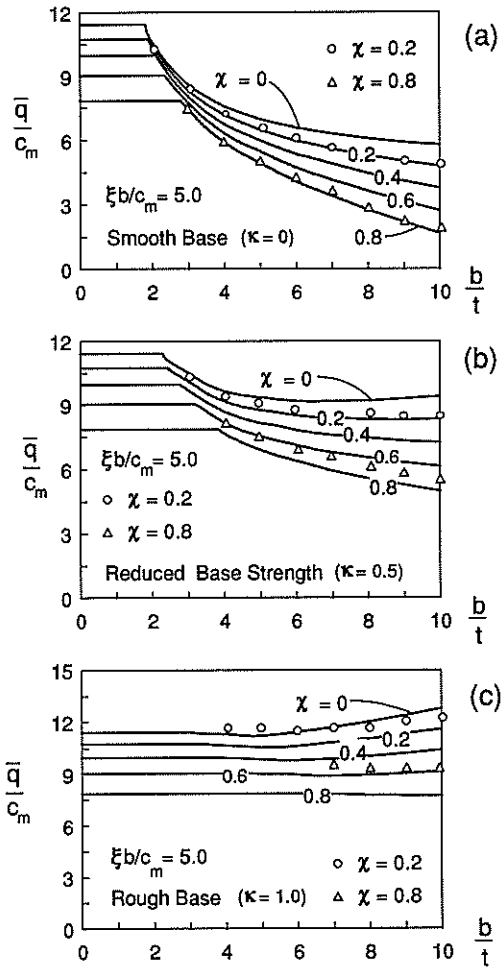

Fig. 5. Limit load $\bar{q}/c_m$ for outward horizontal loads on the foundation layer, strength increasing with depth ($\xi b/c_m=5.0$): (a) smooth base; (b) base strength equal to half of the soil strength at the base; (c) perfectly rough base. Solid lines indicate the numerical solution and bullets mark the closed-form solution

CLOSED-FORM SOLUTION

Limit pressure $\bar{q}/c_m$ over finite thickness layers is dependent on parameters which characterize the horizontal load (χ), base strength ($\kappa=c_b/c$), strength increase with depth ($\xi b/c_m$), and, of course, ratio b/t. Presenting results for a wide range of useful combinations of all parameters would require a large number of diagrams, therefore, an analytical (closed-form) solution was attempted, and it is presented in this section. This analytic solution is attempted here to allow an easy, though less accurate, assessment of limit loads. The analytical solution is based on the mechanisms shown in Figs. 3(a) and 3(c), and is restricted to cases where ratio b/t is equal to natural numbers. The mechanism in Fig. 3(a) is used to derive limit loads for $b/t=2, 4, 6, \cdots$, and the mechanism in Fig. 3(c) is used to obtain the solution for $b/t=1, 3, 5, \cdots$ In both solutions it is assumed *a priori* that angles α and β are equal to $\pi/4$. This is an arbitrary assumption selected so that a closed-form solution could be obtained. As the proc-

ess of optimization of the geometry of the failure mechanism is eliminated, the overestimation of the true limit load is expected to be larger than that in the numerical solution. Only for the particular case where $\kappa=0$ and $\chi=0$ do the two solutions yield identical results. Expressions for dissipation rates and the work rate of external forces are given in the Appendix. Substituting those into eq. (4) makes it possible to solve for the upper bound to $\bar{q}/c_m$

$$\frac{\bar{q}}{c_m}=3+\frac{\pi}{2}+\frac{1}{2}\frac{b}{t}(\kappa-\chi)+\frac{\xi b}{c_m}\left[\frac{t}{b}(1+\sqrt{2})+\frac{\kappa}{2}\right],\quad \frac{b}{t}=2,\ 4,\ 6,\cdots \tag{12}$$

for the mechanism in Fig. 3(a), and

$$\frac{\bar{q}}{c_m}=3+\frac{\pi}{2}+\frac{1}{2}\frac{b}{t}(\kappa-\chi)+\frac{1}{2}\frac{t}{b}(\kappa+\chi)+\frac{\xi b}{c_m}\left[\frac{t}{b}(1+\sqrt{2})+\frac{\kappa}{2}\left(1+\frac{t^2}{b^2}\right)\right],\quad \frac{b}{t}=1,\ 3,\ 5,\cdots \tag{13}$$

for the mechanism in Fig. 3(c).

Limit loads obtained from the analytical solution (Eqs. (12) and (13)) are presented in Figs. 4 and 5 as small circles for horizontal load intensity $\chi=0.2$, and as triangles for $\chi=0.8$. As expected, the closed-form solution yields higher limit loads than the numerical one does. For a smooth base ($\kappa=0$) and $\chi=0.2$, the analytical solution overestimates the numerical one by less than 0.3% ($b/t\leq 10$). The overestimation becomes higher when χ increases and is greatly influenced by the strength of the base (see Figs. 4 and 5).

As the analytical solution (Eqs. (12) and (13)) is strictly valid only for b/t equal to integers, this solution should be interpolated for b/t other than integers. Since the analytical solution is a continuous function of ratio b/t, the interpolation can be performed by substituting the required value of b/t (a positive real number) directly into Eq. (12) or Eq. (13). While substitution of b/t with values other than integers contradicts the assumptions used to derive Eqs. (12) and (13), it should be viewed only as an interpolation technique.

CRITICAL EMBANKMENT HEIGHTS AND INFLUENCE OF REINFORCEMENT

Numerical and analytical results were shown in previous sections for horizontal load intensity $\chi>0$, as the thrust in the embankment causes an outward horizontal load on the foundation soil. The solutions presented, however, also are valid for cases where the horizontal forces transmitted to the soil during collapse are directed inward; such forces are known to exist under rough footings. Horizontal inward forces are also conceivable under reinforced embankments, where during collapse of the foundation layer the embankment does not follow the displacements of that layer, as the reinforcement constrains the lateral spreading of the embankment.

Fig. 6 represents selected numerical and analytical results for layers loaded with inward horizontal loads, typical of reinforced embankments. The analytical solution represented by Eqs. (12) and (13) now yields results almost identical to the numerical one, independent of whether the layer is resting on a smooth or rough base.

The total thrust (horizontal force) in the embankment at the symmetry plane can be estimated as $\gamma_f H^2 K/2$, where H is the embankment height, γ_f is the unit weight of the embankment fill, and K is the coefficient of lateral pressure. For unreinforced embankments, this thrust is transferred to the foundation soil as the outward tangential load characterized by coefficient $\chi=\bar{\tau}/c$. For reinforced embankments, part or all of the thrust is taken over by the reinforcement, and, thus, the tangential load transferred to the foundation soil is likely to be smaller. Assuming that the maximum force in the reinforcement is equal to its tensile strength (implying tensile failure rather than pull-out), coefficient χ can be calculated as

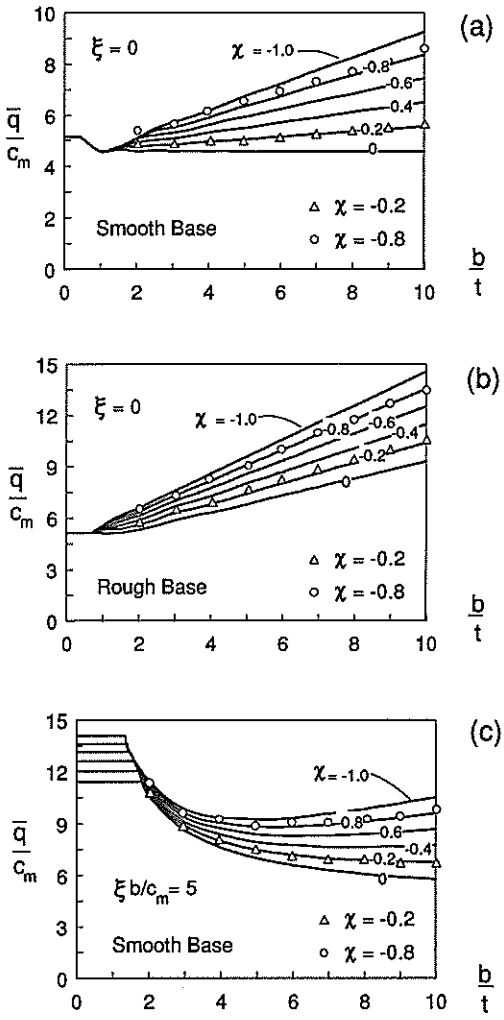

Fig. 6. Limit load $\bar{q}/c_m$ for inward horizontal loads on the foundation layer: (a) smooth base, homogeneous soil; (b) perfectly rough base, homogeneous soil; (c) smooth base, strength increasing with depth ($\xi b/c_m=5.0$). Solid lines indicate the numerical solution and bullets mark the closed-form solution

$$\chi=\frac{\bar{\tau}}{c_m}=\frac{\gamma_f H^2 K-2R}{2bc_m} \tag{14}$$

where R is the tensile strength of the reinforcement (or, for practical purposes, a tensile force at some specified allowable lateral embankment strain) per unit length of the embankment. Coefficient of lateral pressure K cannot be smaller than $\tan^2(\pi/4-\varphi_f/2)$ ($K=(1-\sin\varphi_f)$ is recommended for conservative design). It is conceivable that, if the reinforcement is strong enough, the soil is displaced laterally during collapse of the foundation soil layer (e.g., according to the mechanism in Fig. 3(a)), while the embankment does not spread, due to being constrained by the reinforcement. In such case horizontal forces acting on the foundation layer are directed inward ($-1\le\chi<0$).

It needs to be emphasized that, under working conditions, coefficient χ is likely to be positive. Only at the onset of failure, when the soft soil begins to be "squeezed out" from underneath the embankment (incipient failure), may the total thrust in the embankment be equilibrated by the force in the reinforcement, and further increase in the reinforcement force due to movement of the foundation soil with respect to the fill may cause inward horizontal forces (negative χ). Such a state may be allowed to persist under embankments over soft soils until the consolidation process, caused by the surcharge load (embankment weight), leads to an increase in the foundation strength.

Critical heights of embankments over cohesive soil layers can be estimated using the respective diagrams, or using Eqs. (12) and (13). To make use of these diagrams and formulae, coefficient χ first has to be estimated from Eq. (14). The limits on χ are -1.0 and 1.0. The embankment for which $\chi=-1.0$ is referred to as a *fully reinforced embankment*. An increase in the amount of reinforcement beyond that assuring $\chi=-1.0$ does not lead to an increase in critical height (or the safety factor). Once χ is calculated from Eq. (14), the particular diagram or formula can be used to determine $\bar{q}/c$. Since the total vertical force under one half of the embankment, $\bar{q}b$, must be equal to the weight of the fill, $\gamma_f(bH-H^2\cot\delta/2)$, the critical (failure) height can be calculated as

$$H=b\tan\delta\left(1-\sqrt{1-\frac{2\bar{q}}{b\gamma_f\tan\delta}}\right) \tag{15}$$

where δ is the slope angle. Note that χ is a function of H, therefore the process of finding the critical embankment height is iterative. If $\bar{q}$ becomes large enough so that the function

under the square root becomes negative, the embankment height becomes limited by its maximum value of $b \tan \delta$. Alternatively, as suggested in the literature (e.g., Bonaparte et al. 1987; Rowe and Soderman, 1987), the computational width of the embankment can be taken at its mid-height and the failure height can be calculated as $H = \bar{q}/\gamma_f$.

DISCUSSION

Numerical and analytical (closed-form) solutions were shown for the bearing capacity of finite thickness layers of cohesive soil over rigid bases. These solutions account for a horizontal, uniformly distributed load of arbitrary intensity; they also account for an increase in the soil strength with depth and different shear strengths of the bases. The analysis was performed with the design of embankments in mind, where the intensity of the horizontal load on the foundation soil depends on the embankment height and on whether or not reinforcement is used.

A comparison of the solutions presented in this paper to those by Mandel and Salençon (1972) and by Matar and Salençon (1977) is shown in Fig. 7 for both smooth and rough bases, for uniform strength, and for strength increasing with depth (note that in this paper b is the half-width of the embankment, while in the other papers B denotes the total width). As expected, the solutions for rough footings based on the method of characteristics compare very well to those presented in this paper for large inward horizontal loads typical to fully reinforced embankments (χ close to -1.0). Note that in solutions using the slip-line method, the average intensity of the horizontal load, χ, does not reach -1.0 ($\chi = -1.0$ along BEG, Fig. 1, and χ drops to 0 at point O).

An extension of the admissible stress field in the layer beyond the loaded area can be found for solutions by Mandel and Salençon, and Matar and Salençon. Consequently, these solutions can be proved to be rigorous lower bounds to the true limit load. It may very well be that they are exact solutions, since associated kinematically admissible failure mechanisms can be found. For these solutions to be exact the work dissipation rate needs to be proved non-negative everywhere in the deformation field. As the solutions are numerical in nature, there is no easy way to prove this. Hence, the solutions by the method of characteristics are cautiously considered here as lower bound solutions, and are used as verification of the upper bounds obtained in

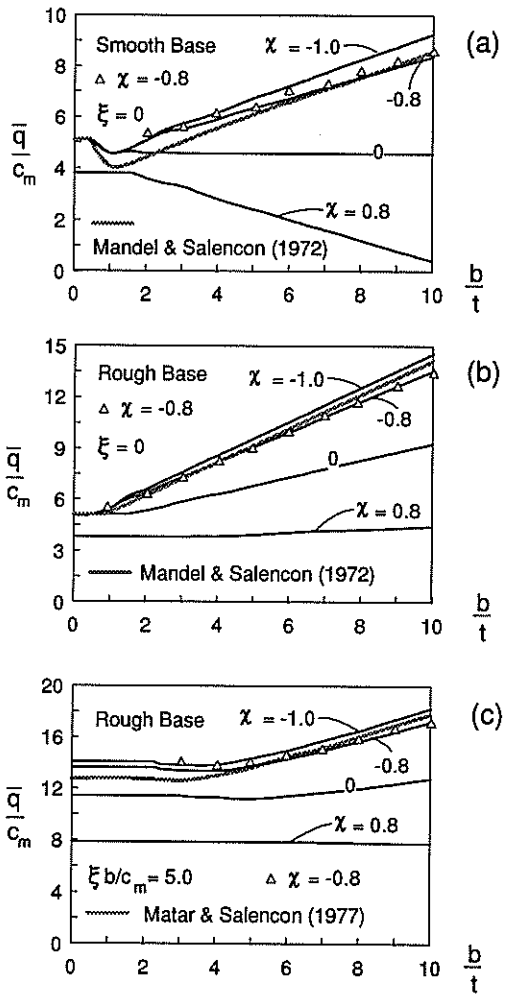

Fig. 7. Comparison of proposed solutions to those of Mandel and Salençon (1972) and Matar and Salençon (1977) for rough footings: (a) smooth base, uniform soil strength; (b) rough base, uniform soil strength; (c) rough base, strength increasing with depth ($\xi b/c_m = 5.0$). Solid lines indicate the numerical solution and bullets mark the closed-form solution for $\chi = -0.8$

this paper. The advantage of the solutions presented here is in much simpler calculations, especially when strength increase with depth is to be accounted for. Fig. 7 indicates that the solutions presented are especially accurate for important practical cases: layers over rough bases and a large inward-acting horizontal load (characteristic of fully reinforced embankments). The more general conclusion is that the rigid-block collapse mechanism used in the analysis is flexible enough to yield the least upper bound very close (within a few percent) to the lower bound solution. Work is underway to obtain slip-line solutions for an arbitrary intensity of the horizontal load. The preliminary calculations indicate that the numerical solutions presented in this paper overestimate the ones from the slip-line method to about the same extent as in the cases in Fig. 7.

The collapse mechanism used to derive the closed-form solution is more restrictive, as angles α and β (Fig. 3(a) and Fig. 3(c)) were both fixed at $\pi/4$; therefore the analytical solution has a higher overestimation margin. This solution should be regarded as a more approximate, but convenient tool for rough estimates of the limit loads.

The solutions presented in this paper are rigorous upper bounds to the true value of the average limit vertical pressure, where the magnitude of the horizontal load component and its distribution are given; this horizontal load is not part of the solution. When it comes to application of these solutions in the design of embankment heights, the horizontal load transmitted from the embankment to the soil has to be estimated. While the total horizontal load transmitted to the foundation soil under one-half of the embankment can be estimated assuming, for example, an active or at-rest stress state in the embankment, its distribution is not known. For lack of better data, uniform distribution was assumed here. Such distribution was also assumed by others in a solution to bearing capacity of the half-space under embankments (Houlsby and Jewell, 1988). If the intensity of the horizontal load is assumed to decrease from the center of the embankment toward the slopes, then the solutions based on mechanisms considered here will lead to larger limit loads when the horizontal force is outward, and smaller limit loads when the horizontal force is inward. The opposite is true when the intensity of the horizontal load increases with the distance from the center of the embankment. The uniform distribution was used here when considering the bearing capacity type of failure under the entire embankment. Less favorable distributions are likely to cause a partial embankment failure, and such distributions are indirectly accounted for in analyses of embankment slope failure and embankment "spreading", not covered in this paper.

CONCLUSIONS

(a) Solutions to the bearing capacity of finite thickness layers under rough footings, based on the slip-line method, lead to overestimation of the bearing capacity when used in the design of unreinforced embankments.

(b) The numerical solution presented is based on collapse mechanisms leading to results within a few percent of the lower bound solutions available in the literature for nearly-full mobilization of inward-acting horizontal forces. It is expected to be equally reliable for other horizontal loads, as the minimization technique allows the mechanism adjustment to account for the most adverse effect of the horizontal load. The closed-form solution should be used with caution.

(c) For thick foundation layers or narrow embankments (small ratios b/t), a failure mechanism may occur which does not reach the base of the layer; a solution based on the classical Hill (or Prandtl) collapse mechanism is appropriate in such case.

(d) Failure of the foundation soil under the entire width of the fill is only one possible mode of embankment collapse. Failures under a smaller portion of the fill, rotational embankment slope failures, and "spreading", not presented in this paper, also need to be analyzed in the entire design process.

REFERENCES

1) Bonaparte, R., Holtz, R. D. and Giroud, J. P. (1987): "Soil reinforcement design using geotextiles," Symposium on Geotextiles, Geomembranes and Related Products, ed. J. E. Fluet, LA, 1985.
2) Collins, I. F. (1969): "The upper bound theorem for rigid/plastic solids generalized to include Coulomb friction," J. Mech. Phys. Solids, Vol. 17, pp. 323–338.
3) Davis, E. H. and Booker, J. R. (1973): "The effect of increasing strength with depth on the bearing capacity of clays," Géotechnique, Vol. 23, pp. 551–563.
4) Drucker, D. C., Greenberg, H. J. and Prager, W. (1952): "Extended limit design theorems for continuous media," Q. Appl. Math., Vol. 9, pp. 381–389.
5) Hill, R. (1950): Mathematical Theory of Plasticity, Oxford.
6) Houlsby, G. T. and Jewell, R. A. (1988): "Analysis of unreinforced embankments on soft clays by plasticity theory," in Numerical Methods in Geomechanics, ed. Swoboda, Innsbruck 1988, pp. 1443–1448.
7) Humphrey, D. N. and Holtz, R. D. (1986): "Reinforced embankments—A review of case histories". Geotextiles and Geomembranes, Vol. 4, pp. 129–144.
8) Izbicki, R. J. and Mrōz, Z. (1976): Limit Analysis Methods in the Mechanics of Soils and Rocks, (in Polish) PWN.
9) Jewell, R. A. (1988): "The mechanics of reinforced embankments on soft soils," Geotextiles and Geomembranes, pp. 237–273.
10) Jürgenson, L. (1934): "The application of elasticity and plasticity to foundation problems," J. Boston Soc. Civ. Eng., Vol. 21, pp. 206–241.
11) Leshchinsky, D. (1987): "Short-term stability of reinforced embankment over clayey foundation," Soils and Foundations, Vol. 27, No. 3, pp. 43–57.
12) Mandel, J. and Salençon, J. (1972): "Force portante d'un sol une assise rigide (étude théorique)". Géotechnique, London, England, Vol. 22, No. 1, pp. 79–93.
13) Matar, M. and Salençon, L. (1977): "Capacité portante a une semelle filante sur sol purement cohérént d'épaisseur limitée et de cohésion variable avec la profondeur," Annales de l'Institute Technique du Batiment et des Travaux Publics, Suplément No. 352, Serie: Sols et Fondations, Vol. 143, pp. 95–107.
14) Michalowski, R. L. (1992): "Bearing capacity of nonhomogeneous cohesive soils under embankments," J. Geot. Eng., Vol. 118, No. 7, pp. 1098–1118.
15) Rowe, R. K. and Soderman, K. L. (1987): "Stabilization of very soft soils using high strength geosynthetics: the role of finite element analyses," Geotextiles and Geomembranes, Vol. 6, pp. 53–80.
16) Silvestri, V. (1983): "The bearing capacity of dikes and fills founded on soft soils of limited thickness." Can. Geot. J., Vol. 20, pp. 428–436.
17) Sokolovski, V. V. (1965): "Statics of Granular Media," Pergamon.

APPENDIX

The work dissipation rate in the incipient failure mechanisms shown in Figs. 3(a) and 3(c), where both angles α and β are assumed equal to $\pi/4$, are given below. Note that assuming fixed values of α and β restricts ratios b/t to integer numbers ($b/t=2, 4, 6\cdots$ for the mechanism in Fig. 3(a), and $b/t=1, 3, 5\cdots$ for the mechanism in Fig. 3(c)). The work dissipation rate along all discontinuity surfaces in area OAED can be written as

$$\dot{D}_{\mathrm{OAED}}=bV^0c_m\left(2+\frac{\xi t}{c_m}\right) \tag{16}$$

along discontinuity EG

$$\dot{D}_{\mathrm{EG}}=\frac{\pi}{4}bV^0c_m\left(1+\frac{2\sqrt{2}}{\pi}\frac{\xi t}{c_m}\right) \tag{17}$$

along GH

$$\dot{D}_{\mathrm{GH}}=bV^0c_m\left(1+\frac{\sqrt{2}}{4}\frac{\xi t}{c_m}\right) \tag{18}$$

and within area DEG

$$\dot{D}_{\mathrm{DEG}}=\frac{1}{4}bV^0c_m\left(\pi+\sqrt{2}\frac{\xi t}{c_m}\right) \tag{19}$$

The work rate of the vertical (unknown) average pressure $\bar{q}$ is also the same for both mechanisms, and is equal to

$$\dot{W}_q=b\bar{q}V^0 \tag{20}$$

The energy dissipation rate along the base interface and the work rate of the horizontal load component τ (uniformly distributed), however, is expressed differently for the two mechanisms. The respective expressions are

$$\dot{D}_{\mathrm{AE}}=\frac{\kappa}{2}bV^0c_m\frac{b}{t}\left(1+\frac{\xi t}{c_m}\right) \tag{21}$$

and

$$\dot{W}_\tau=\frac{\chi}{2}bV^0c_m\frac{b}{t} \tag{22}$$

for the mechanism in Fig. 3(a), and

$$\dot{D}_{AE}=\frac{\kappa}{2}bV^0c_m\left(\frac{b}{t}+\frac{t}{b}\right)\left(1+\frac{\xi t}{c_m}\right) \tag{23}$$

and

$$\dot{W}_\tau=\frac{\chi}{2}bV^0c_m\left(\frac{b}{t}-\frac{t}{b}\right) \tag{24}$$

for the mechanism in Fig. 3(c). The above expressions were substituted in Eq. (4) to derive closed-form solutions shown as Eqs. (12) and (13). (Note that $D_v=D_{DEG}$, $D_L=D_{OAED}+D_{EG}$, $D_{Lb}=D_{AE}$, $W_Q=W_q+W_\tau$, and $W_\gamma=0$.)

NOTATION

The following symbols are used in the paper:

b = half-width of the embankment
c = cohesion or undrained shear strength
c_b = shear strength of the base interface
c_m = minimum value of shear strength of soil (at surface)
$\dot{D}_L$ = work dissipation rate along velocity discontinuities
$\dot{D}_{Lb}$ = work dissipation rate along the base interface
$\dot{D}_v$ = work dissipation rate in continually deforming soil
H = embankment height
K = coefficient of lateral pressure
n = parameter indicating the number of moving blocks within a layer under the loaded area
$\bar{q}$ = average vertical limit pressure over foundation soil layer
Q_i = stress vector along a loaded boundary
R = tensile strength of reinforcement per unit length of embankment
t = layer thickness
V_i = velocity vector
$[V]_i$ = velocity jump across a discontinuity
$\dot{W}_Q$ = work rate of external load Q_i
$\dot{W}_\gamma$ = work rate of the body forces
α = geometrical parameter (angle) of the failure mechanism
β = geometrical parameter
γ_f = unit weight of embankment fill
δ = slope inclination angle
κ = base strength c_b over shear strength of the soil at the base interface (c_b/c)
ξ = parameter describing the increase of strength with depth (strength gradient)
χ = horizontal load intensity or coefficient of mobilization of shear stress along the embankment fill-foundation soil interface ($\chi=\bar{\tau}/c$)
ψ = geometrical parameter (angle) of the failure mechanism
$\bar{\tau}$ = average shear stress on the embankment fill-foundation soil interface
φ_f = internal friction angle of embankment fill